Supporting Information for

A High-Efficiency and Long-Cycling Aqueous Indium Metal Battery Enabled by Synergistic In^{3+}/K^{+} Interactions

Songyang Chang,[a] Wentao Hou,[a] Amanda Conde-Delmoral,[a] Irfan Ullah,[a] Jose Fernando Florez Gomez,[b] Gerardo Morell,[b] and Xianyong Wu[a]*

S. Chang, W. Hou, A. Conde-Delmoral, I. Ullah, X. Wu
Department of Chemistry, University of Puerto Rico-Rio Piedras Campus, San Juan, PR 00925-2537, USA
E-mail: xianyong.wu@upr.edu

J. F. Florez Gomez, G. Morell
Department of Physics, University of Puerto Rico-Rio Piedras Campus, San Juan, PR, 00925-2537, USA

Experimental methods

1. Material synthesis

We synthesized the $FeFe(CN)_6$ material based on a simple liquid precipitation method. Typically, we added the $K_3Fe(CN)_6$ solution (40 mL, 0.1 M) to the $FeCl_3$ solution (80 mL, 0.1 M) under magnetic stirring, and we kept the drak brown solution stirring at 60°C for 6 hours. After reaction, the solution was cooled down to the room temperature, and we collected the dark green precipitates by washing and centrifugation. These powders were further dried in an oven at 60°C.

2. Physical characterization

The XRD pattern of the $FeFe(CN)_6$ material was tested on the Rigaku SuperNova equipped with a HyPix3000 X-ray detector and Cu-Kα radiation source (λ = 1.5406 Å). The SEM images and EDS mapping were recorded at a field emission scanning electron microscope (SEM, JEOL, JSM-6480LV).

3. Electrode preparation

The $FeFe(CN)_6$ electrode consisted of the $FeFe(CN)_6$ powders, Ketjen black carbon, and polyvinylidene fluoride (PVDF) binder in a mass ratio of 7:2:1. The composites were well dispersed in the N-Methyl-2-pyrrolidone (NMP) solvent, and the slurry was cast on carbon fiber papers (Fuel Cell Store, AvCarb MGL370, 0.37 mm in thickness, and 1 cm in diameter). The active mass loading is 1.5-2.0 mg cm^{-2}. The self-standing $FeFe(CN)_6$ electrode was composed of the $FeFe(CN)_6$ powders, Ketjen black carbon, and the polytetrafluoroethylene (PTFE) binder in 7:2:1 mass ratio, with an active mass loading of ~5 mg cm^{-2}.

4. Battery assembly and testing

The symmetrical In-In batteries were assembled in 2032 coin cells, with two indium metal foils (99.99% purity, 0.2 mm thickness) sandwiched by glass fiber separators. The asymmetrical In-Ti batteries were also fabricated in 2032 coin cells, wherein a high-purity Ti foil (0.03 mm thickness) worked as the substrate and an In metal foil as the counter electrode. The electrolyte is an aqueous 1.0 m $InCl_3$ + X m KCl solution (X = 0, 1, 2, 3, and 4.5), and the electrolyte volume is 100 μL. The In-$FeFe(CN)_6$ batteries were assembled in Swagelok cells, which used anti-corrosion Ti rods as current collectors. To make the In-$FeFe(CN)_6$ full cell, we pre-deposited the In metal on the Ti foil and then disassembled the cell to retrieve the In@Ti electrode (1 mAh cm^{-2}). The Zn-$FeFe(CN)_6$ batteries were assembled in a similar manner.

The Galvanostatic charge-discharge tests were performed on the Landt battery tester (CT3002AU) at room temperature. Cyclic voltammetry curves and electrochemical impedance spectra were obtained on a Biologic SP-150 Potentiostat.

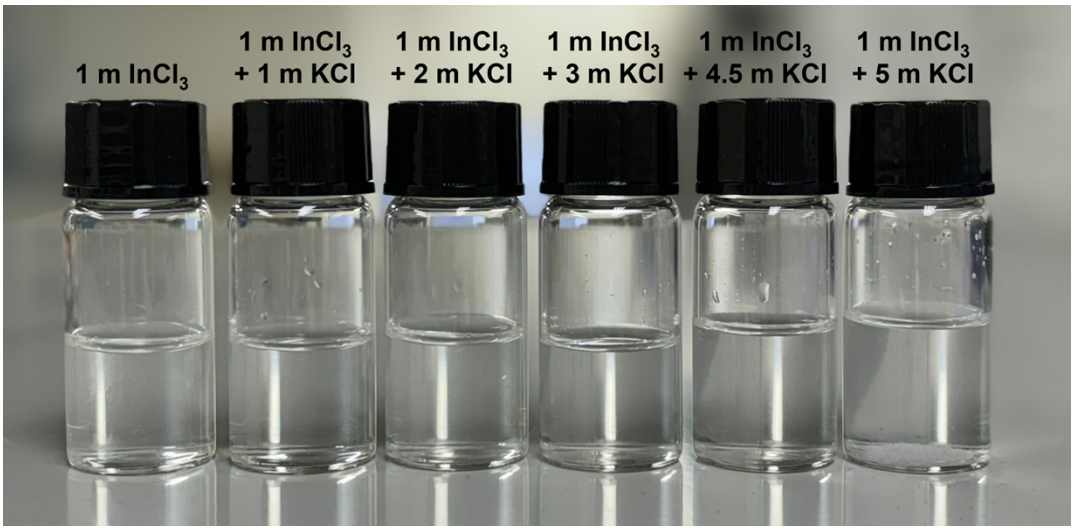

Figure S1. Digital photos of the pure $InCl_3$ electrolyte and KCl+$InCl_3$ hybrid electrolytes.

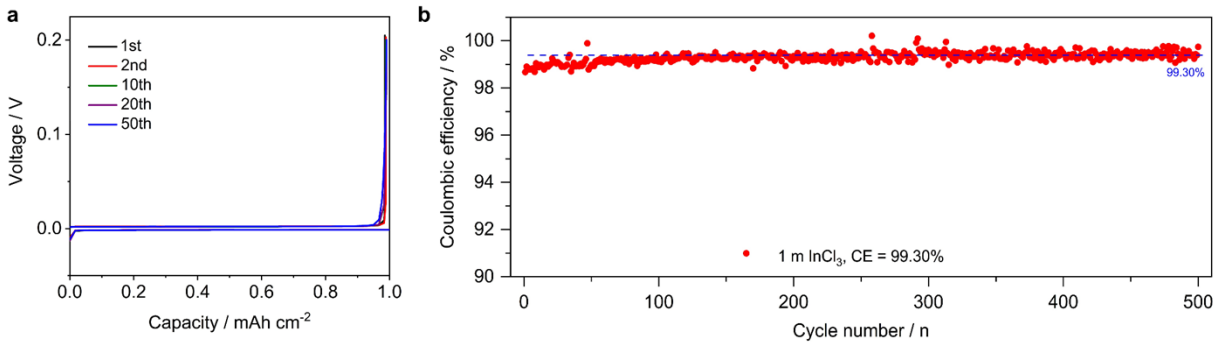

Figure S2. In plating performance in the pristine 1 m $InCl_3$ solution. (a) GCD curves of the In||Ti battery at 1.0 mA cm^{-2} and 1.0 mAh cm^{-2}; (b) The Coulombic efficiency of the In||Ti battery during the cycling.

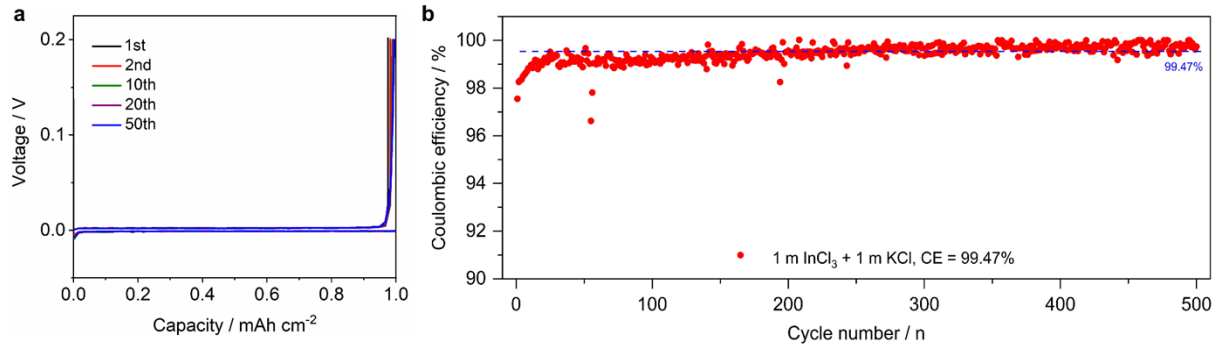

Figure S3. In plating performance in the 1 m $InCl_3$ + 1 m KCl solution. (a) GCD curves of the In||Ti battery at 1.0 mA cm^{-2} and 1.0 mAh cm^{-2}; (b) The Coulombic efficiency of the In||Ti battery during the cycling.

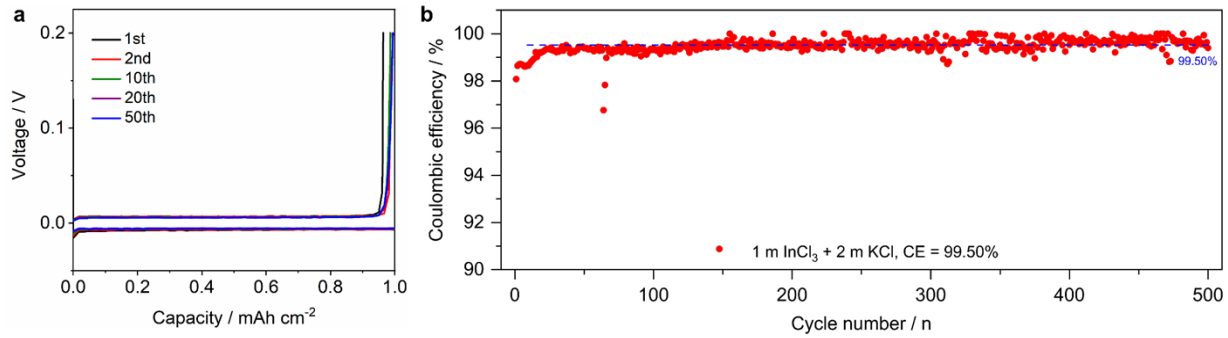

Figure S4. In plating performance in the 1 m $InCl_3$ + 2 m KCl solution. (a) GCD curves of the In||Ti battery at 1.0 mA cm^{-2} and 1.0 mAh cm^{-2}; (b) The Coulombic efficiency of the In||Ti battery during the cycling.

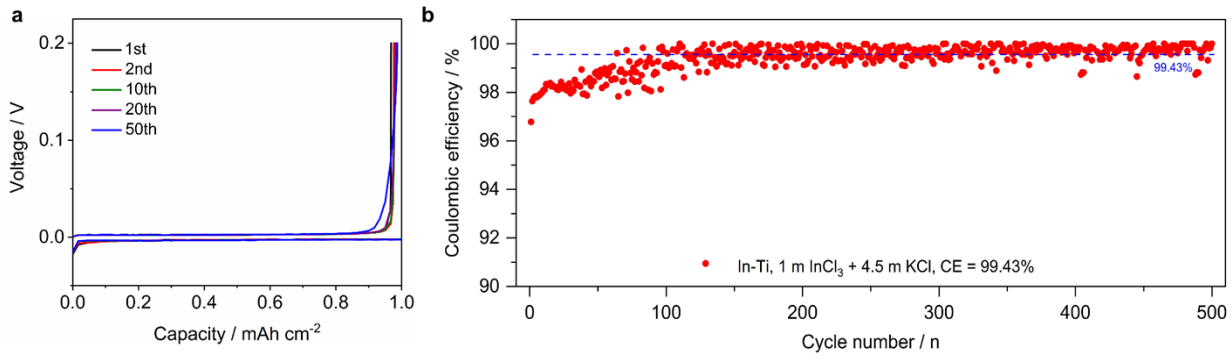

Figure S5. In plating performance in the 1m $InCl_3$ + 4.5 m KCl solution. (a) GCD curves of the In||Ti battery at 1.0 mA cm^{-2} and 1.0 mAh cm^{-2}; (b) The Coulombic efficiency of the In||Ti battery during the cycling.

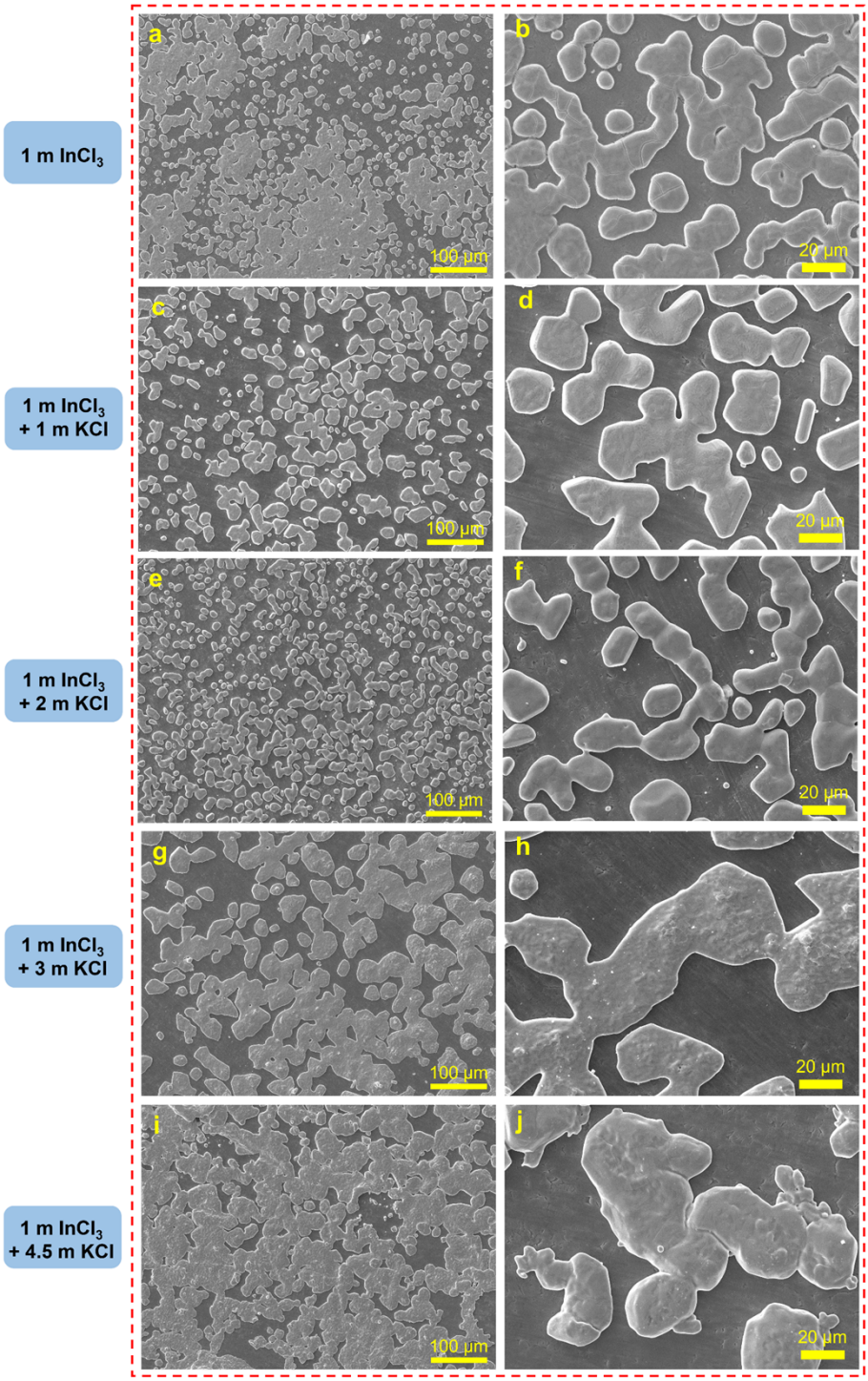

Figure S6. SEM images of the morphology of plated In metals in different electrolytes. (a-b) 1 m $InCl_3$ electrolyte; (c-d) 1 m $InCl_3$ + 1 m KCl electrolyte; (e-f) 1 m $InCl_3$ + 2 m KCl electrolyte; (g-h) 1 m $InCl_3$ + 3 m KCl electrolyte; (i-j) 1 m $InCl_3$ + 4.5 m KCl electrolytes.

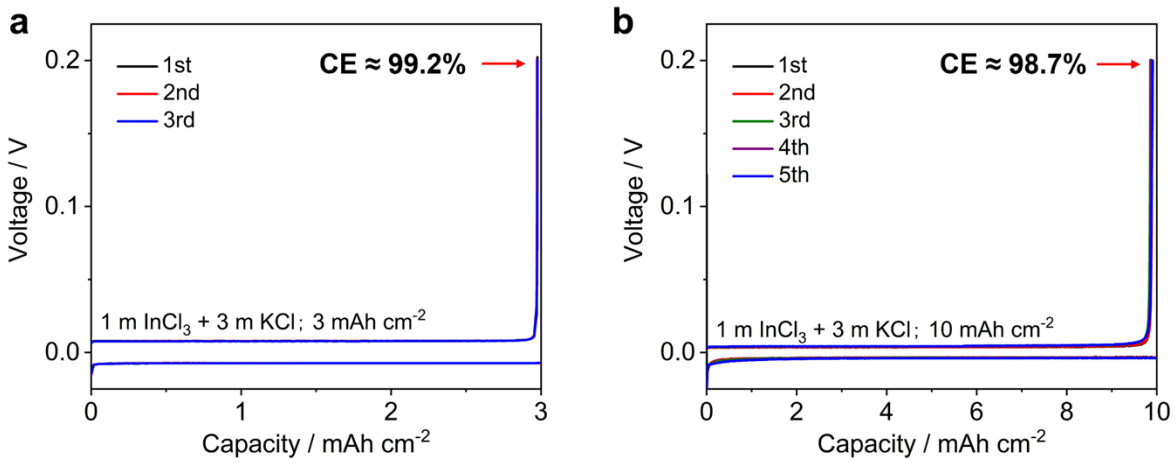

Figure S7. The GCD curves of the In‖Ti battery at higher plating capacities in the 1 m $InCl_3$ + 3 m KCl electrolyte (current density: 1 mAh cm^{-2}). (a) The plating capacity is 3 mAh cm^{-2}; (b) The plating capacity is 10 mAh cm^{-2}.

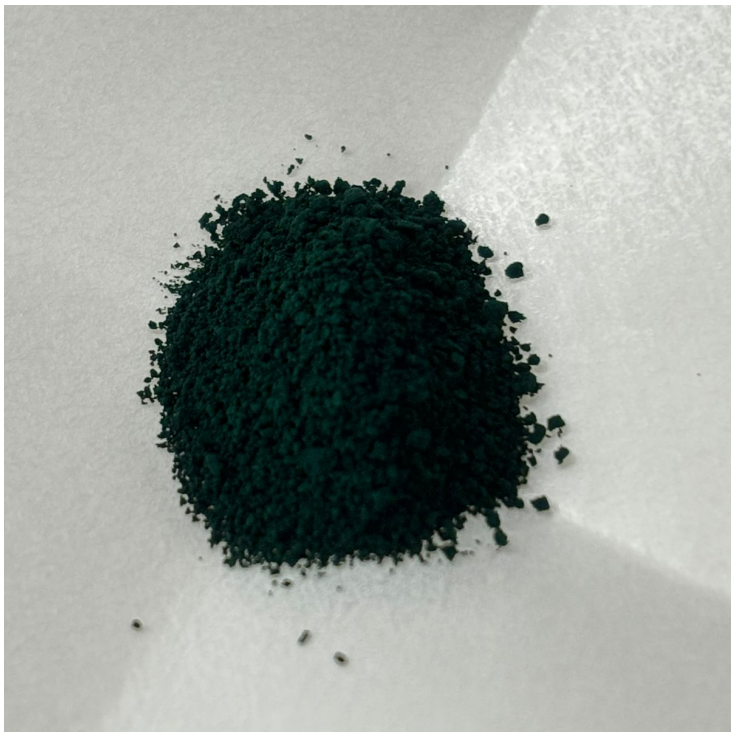

Figure S8. The digital photo of the as-prepared $FeFe(CN)_6$ material.

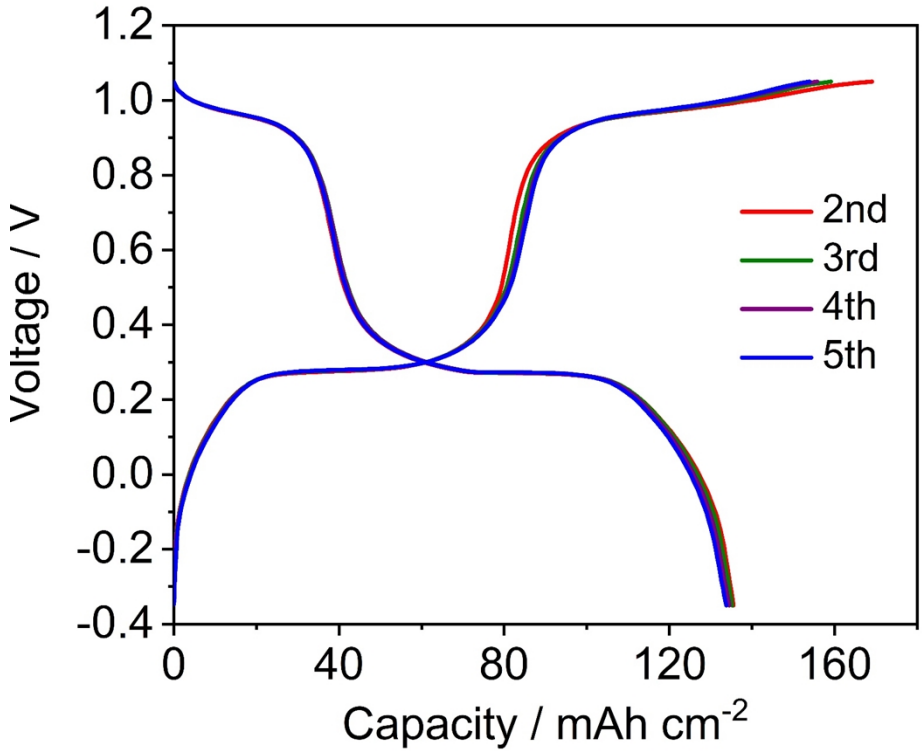

Figure S9. GCD curves of the Ac||$FeFe(CN)_6$ battery in the 3 m KCl electrolyte at 120 mA g^{-1}. The reference electrode is an Ag/AgCl electrode with saturated KCl electrolyte (+0.2 V *vs.* SHE). The counter electrode is a large piece of activated carbon self-standing film.

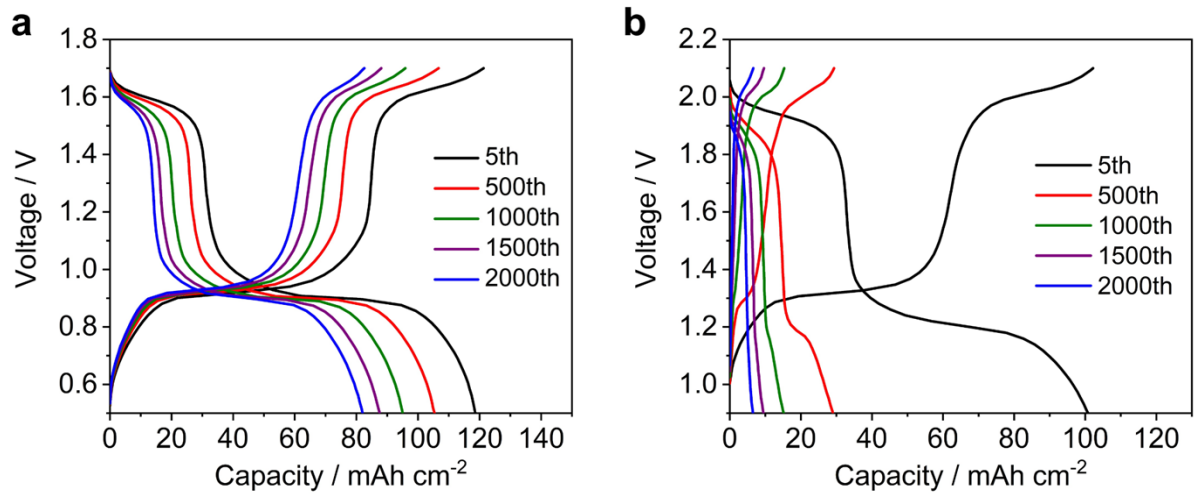

Figure S10. The selected GCD curves of hybrid batteries at 1.2 A g^{-1}. (a) The In||$FeFe(CN)_6$ battery; (b) The Zn||$FeFe(CN)_6$ battery.

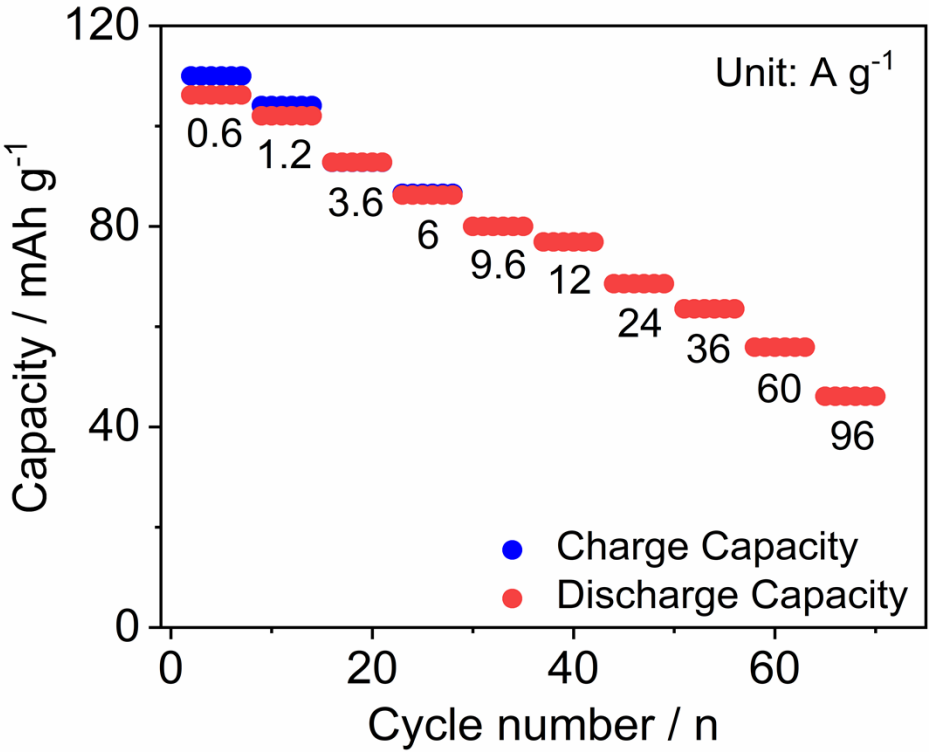

Figure S11. The rate performance of the In||$FeFe(CN)_6$ hybrid battery.

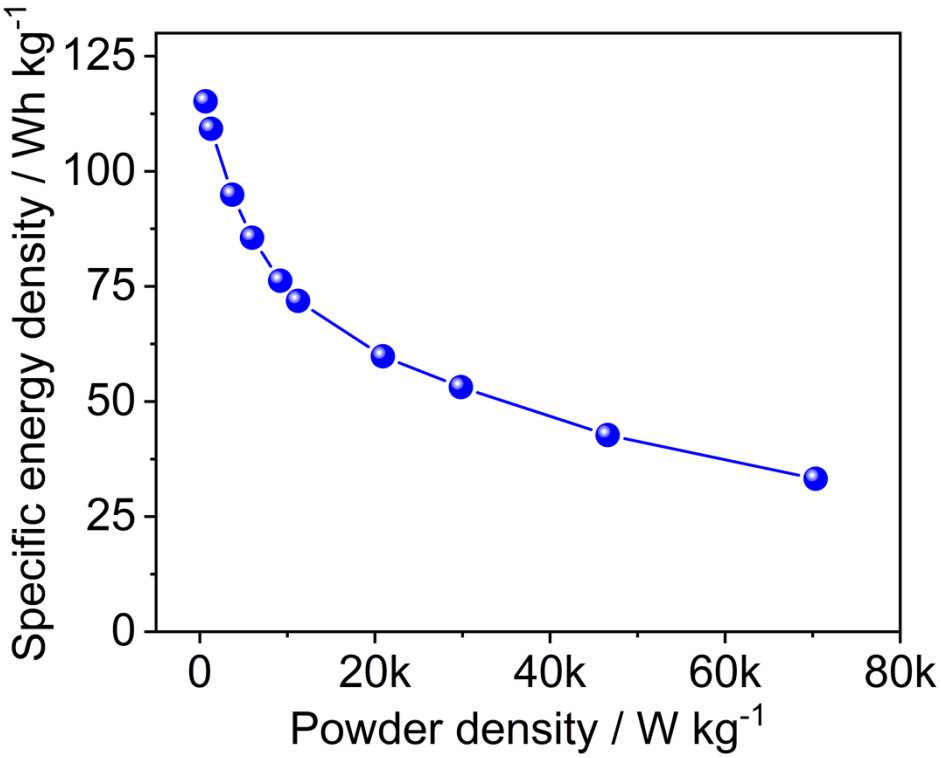

Figure S12. The Ragone plot of the In-$FeFe(CN)_6$ battery.

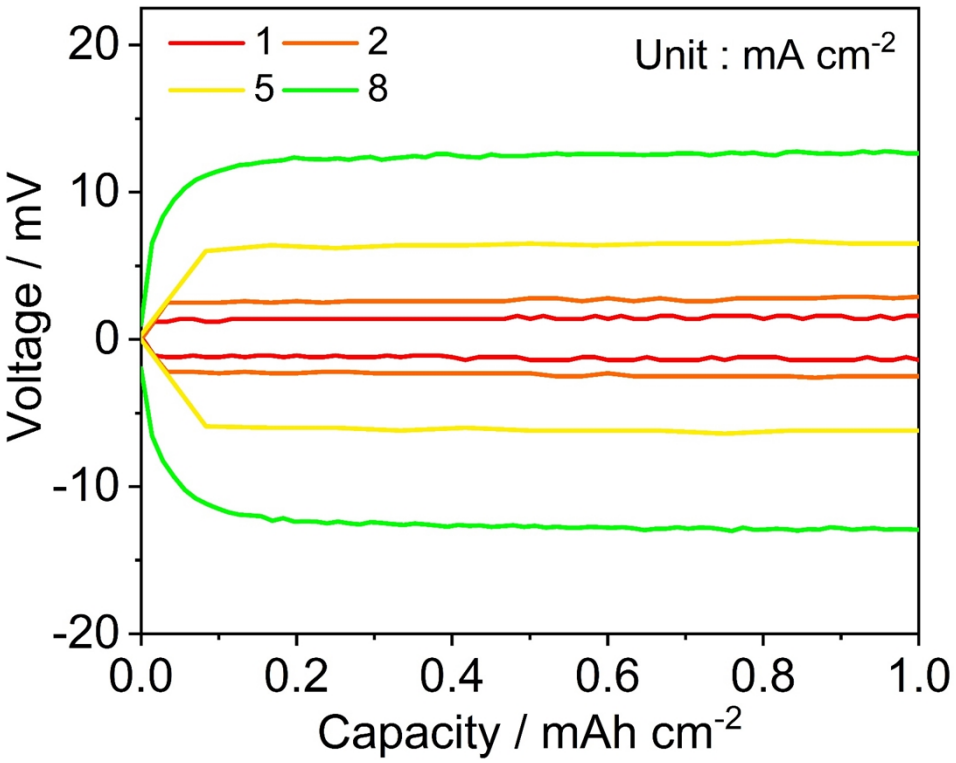

Figure S13. GCD curves of the symmetrical In||In battery at different current densities.

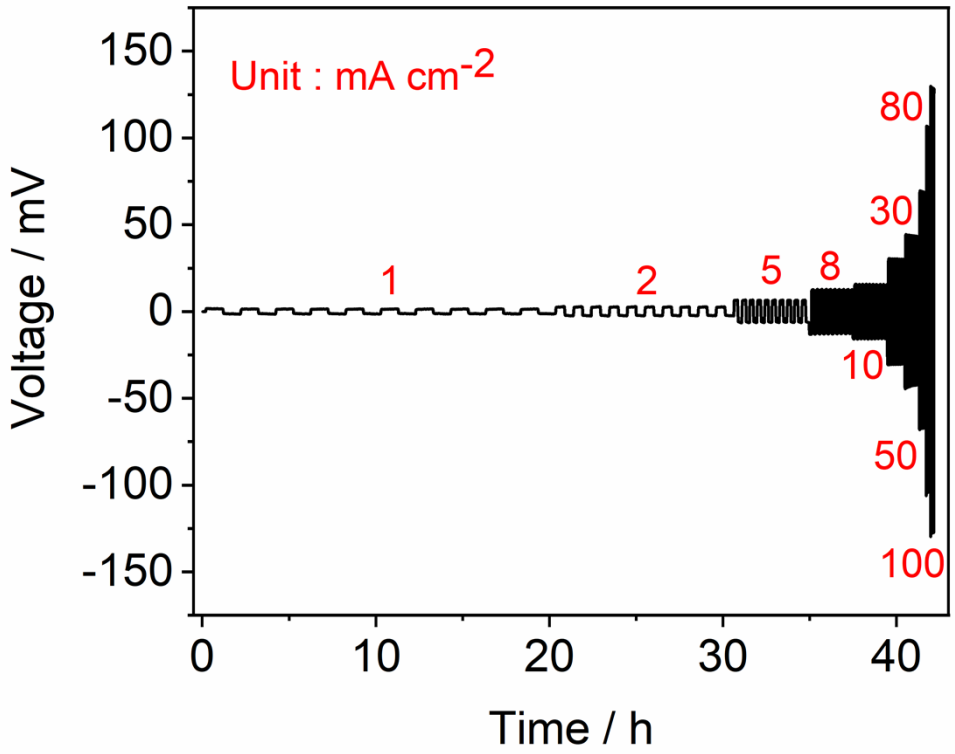

Figure S14. The rate performance of In||In battery in the 1 m $InCl_3$ + 3 m KCl electrolyte.

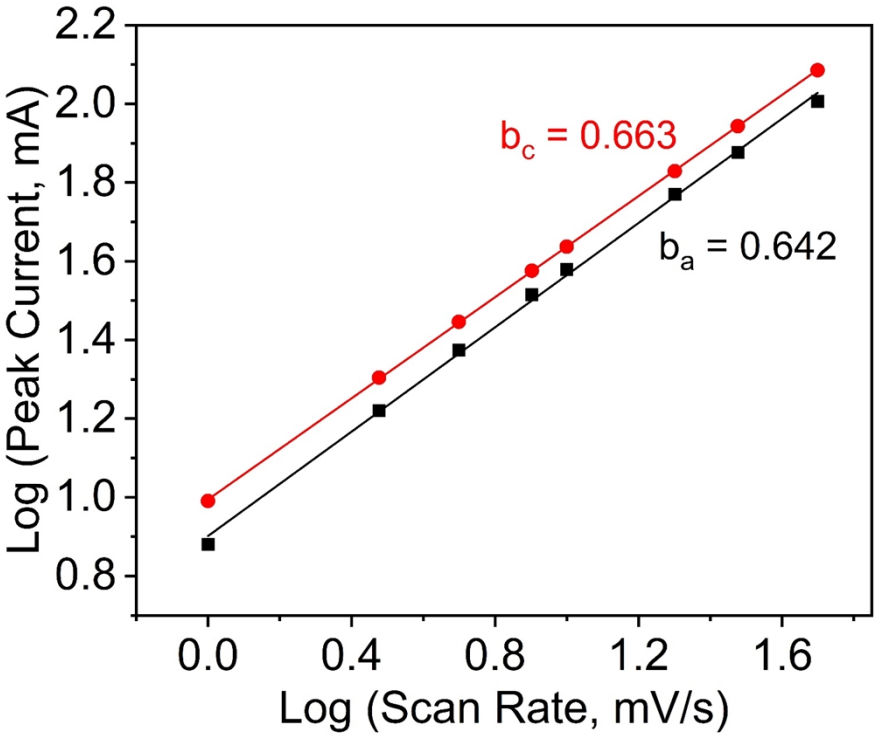

Figure S15. Relationship between the logarithm of peak current [log(i)] and scan rate [log(v)].

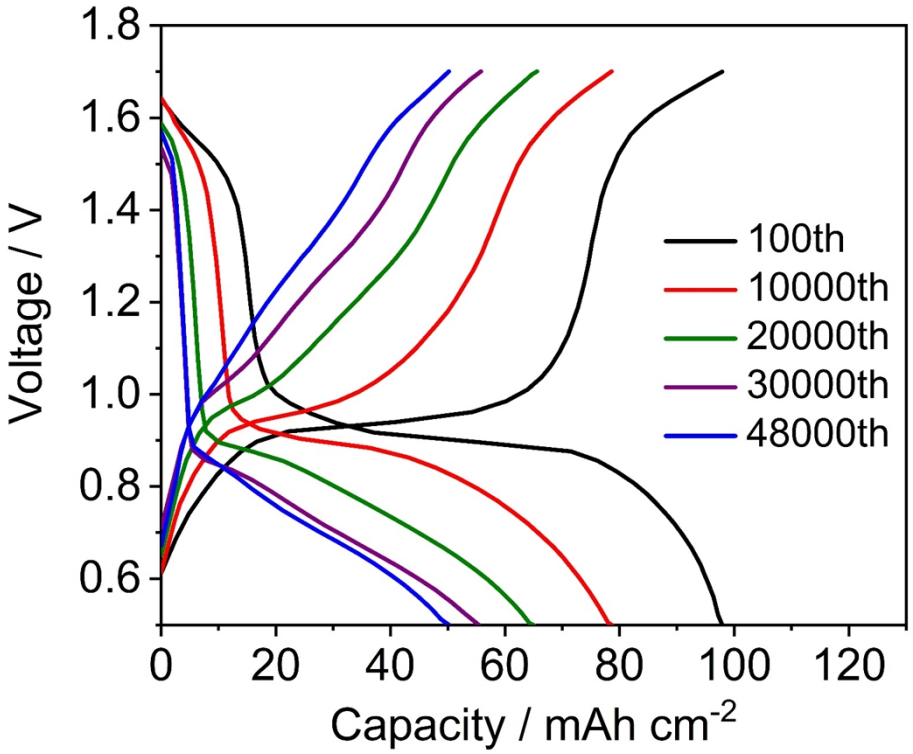

Figure S16. The selected GCD curves of the In||$FeFe(CN)_6$ hybrid battery at 12 A g^{-1}.

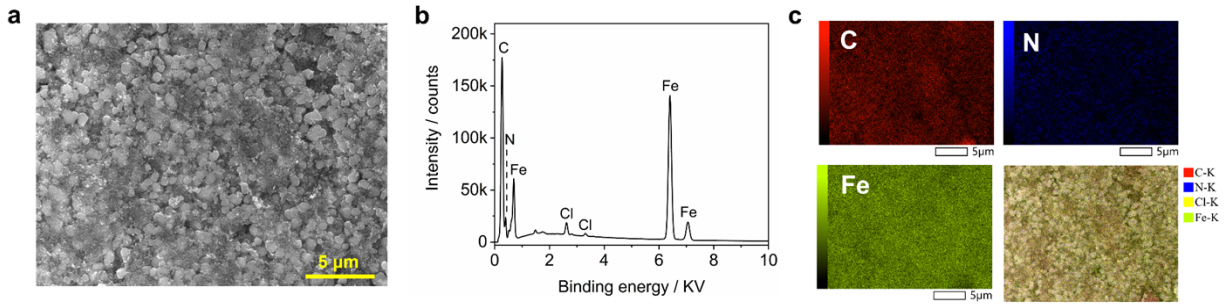

Figure S17. (a) SEM image of the initial $FeFe(CN)_6$ electrode; (b-c) EDS analysis and elemental spectrum results of the initial $FeFe(CN)_6$ electrode.

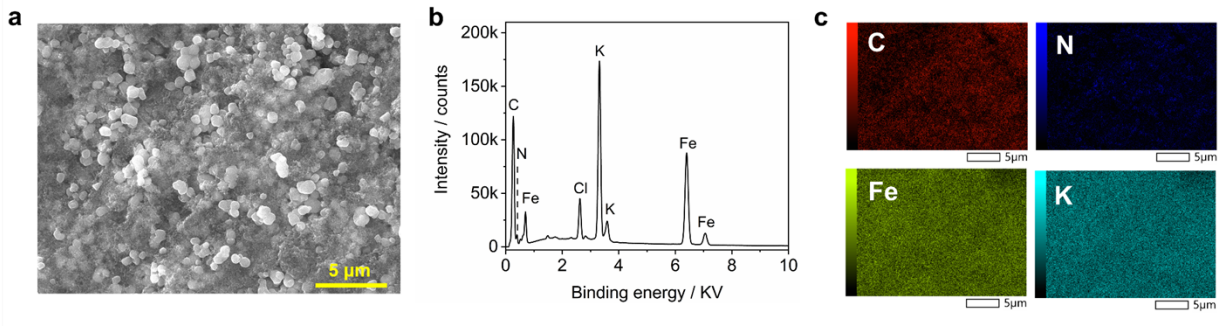

Figure S18. (a) SEM image of $FeFe(CN)_6$ electrode in discharge state; (b-c) EDS analysis and elemental spectrum results of $FeFe(CN)_6$ electrode in discharge state. As shown, after discharge, the K element has significantly increased its content, indicating the reversible K^+ insertion.

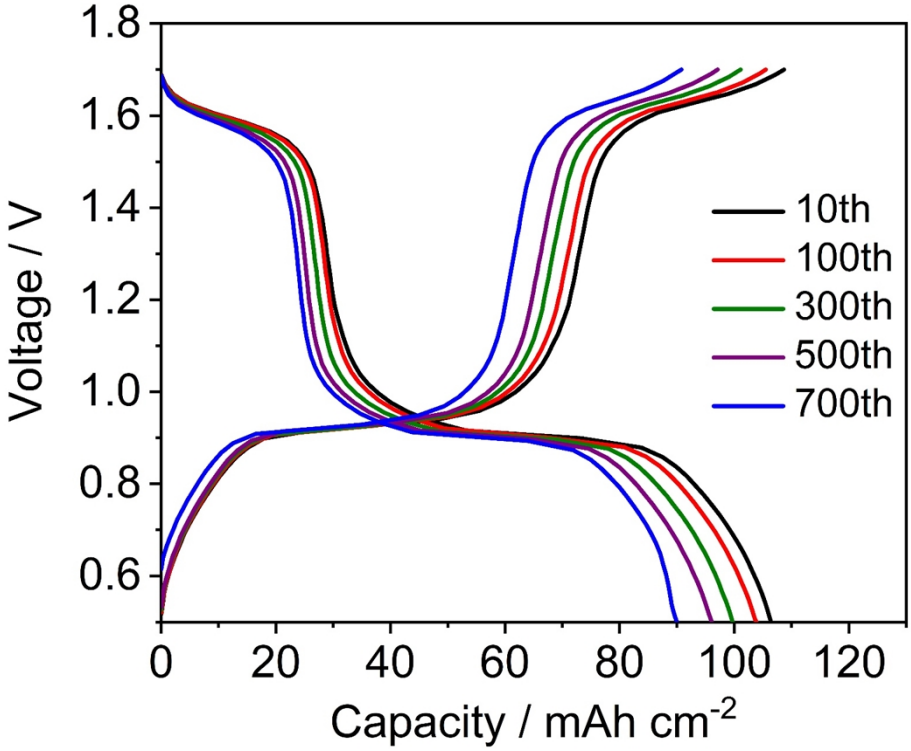

Figure S19. The selected GCD curves of the In||$FeFe(CN)_6$ hybrid full battery at 1.2 A g^{-1}.

Table S1. The cycling performance comparison between our work and literature reports.

Charge carrier	Battery Systems	Cycling, retention	Current rate	Reference
Na^+	Aqueous Na^+ batteries	500, 87%	20C	1
Na^+	Aqueous Na^+ batteries	500, 83%	20C	2
Na^+	Aqueous Zn-Na batteries	200, 84%	15C	3
Na^+	Aqueous Zn-Na batteries	500, 88%	45C	4
Na^+	Non-aqueous Na^+ batteries	100, 84.8%	20 mA g^{-1}	5
Li^+	Non-aqueous Li^+ batteries	300, 90%	24C	6
Al^{3+}	Aqueous Al^{3+} batteries	100, 97.1%	150 mA g^{-1}	7
K^+	Non-aqueous K^+ batteries	500, 93%	5C	8
NH_4^+	Aqueous NH_4^+ batteries	1000, 96.3%	200 mA g^{-1}	9
K^+	Aqueous K-Zn Batteries	1000, 57%	1 A g^{-1}	10
K^+	Non-aqueous K-Zn Batteries	1000, 80.5%	1 A g^{-1}	11
Zn^{2+} /Li^+	Aqueous Zn-Li Batteries	10000, 73%	97C	12
K^+	Aqueous K-In Batteries	1000, 99.2% 10000, 80.7%	100C	This work

References

[1] X. Wu, W. Deng, J. Qian, Y. Cao, X. Ai and H. Yang, *J. Mater. Chem. A*, 2013, **1**, 10130-10134.

[2] X. Wu, Y. Luo, M. Sun, J. Qian, Y. Cao, X. Ai and H. Yang, *Nano Energy*, 2015, **13**, 117-123.

[3] C. Yang, S. Ding, Y. Zhao, J. Zhou, L. Li and J. Fan, *Dalton Trans.*, 2023, **52**, 16984-16992.

[4] C. Yang, Y. Zhao, J. Fan, L. Li, J. Zhou, K. Wang, F. Lu and H. Sun, *Mater. Adv.*, 2024.

[5] F. Maroni, M. Li, S. Dongmo, C. Gauckler, M. Wohlfahrt-Mehrens, M. Giorgetti and M. Marinaro, *ChemElectroChem*, 2023, **10**, e202201070.

[6] X. Wu, M. Shao, C. Wu, J. Qian, Y. Cao, X. Ai and H. Yang, *ACS Appl. Mater. Interfaces.*, 2016, **8**, 23706-23712.

[7] Zhou, L. Jiang, J. Yue, Y. Tong, Q. Zhang, Z. Lin, B. Liu, C. Wu, L. Suo and Y.-S. Hu, *ACS Appl. Mater. Interfaces*, 2019, **11**, 41356-41362.

[8] Z. Shadike, D.-R. Shi, M.-H. Cao, S.-F. Yang, J. Chen and Z.-W. Fu, *J. Mater. Chem. A*, 2017, **5**, 6393-6398.

[9] S. Li, M. Xia, C. Xiao, X. Zhang, H. Yu, L. Zhang and J. Shu, *Dalton Trans.*, 2021, **50**, 6520-6527.

[10] Ni, Z. Hao, G. Y. Zou, F. H. Cao, L. Qin and C. G. Zhou, *ChemElectroChem*, 2022, **9**, e202101351.

[11] G. Ni, M. Sun, Z. Hao, G. Zou, F. Cao, L. Qin, W. Chen and C. Zhou, *Mater. Today Energy*, 2023, **31**, 101204.

[12] Q. Yang, F. Mo, Z. Liu, L. Ma, X. Li, D. Fang, S. Chen, S. Zhang and C. Zhi, *Adv. Mater.*, 2019, **31**, 1901521.